A Numerical Characterisation of Nigerian-Composition CNG Combustion in a Spark-Ignition Direct-Injection Engine

[1]Bamiji Z. Adewole, [2]Ayodele T. Oyeniran, [3]Abdulazeez B. Oni, [4]Samson K. Fasogbon, [5]Adedotun M. Adedoja, [6]Olayinka S. Ohunakin, [7]Abraham A. Asere

[1,2,5,7]Department of Mechanical Engineering, Obafemi Awolowo University, Ile-Ife, Nigeria

[2,3]Department of Aerospace Engineering, Obafemi Awolowo University, Ile-Ife, Nigeria

[4]Department of Mechanical Engineering, University of Ibadan, Ibadan, Nigeria

[5]Department of Mechanical Engineering, Redeemers University, Ede Osun State, Nigeria

[6]The Energy and Environment Research Group (TEERG), Mechanical Engineering Department, Covenant University, Ogun State, Nigeria

[7]Department of Automotive Engineering, Elizade University, Ilara Mokin, Nigeria

bzadewole@oauife.edu.ng|atoyeniran@oauife.edu.ng|abdulazeezoni09@gmail.com |sk.fasogbon@ui.edu.ng| adedojaadedotun@gmail.com|olayinka.ohunakin@covenantuniversity.edu.ng|aaasere77@yahoo.co.uk

Received: 12-JUNE-2026; Reviewed: 29-AUGUST-2026; Accepted: 23-SEPT-2026
https://dx.doi.org/10.46792/fuoyejet.v11i3.1604

ORIGINAL RESEARCH

Abstract—Compressed natural gas (CNG) is a potentially useful gaseous fuel for spark-ignition engines, but its combustion behaviour depends on fuel composition and mixture-formation conditions. This study develops a three-dimensional computational fluid dynamics (CFD) baseline characterisation of Nigerian-composition CNG in a spark-ignition direct-injection (SIDI) research engine. A multi-component natural-gas surrogate representing gas reported for the Utorogu Gas Plant, Nigeria, was implemented in ANSYS Forte. The baseline case used a 0.5 L single-cylinder engine at 2000 rpm and wide-open throttle, with 50 bar CNG injection pressure and start of injection at 310° BTDC. Turbulent flow was represented using the RNG k–ε model, while spark-kernel development and turbulent flame propagation were represented using the discrete particle ignition kernel and G-equation models. The model was evaluated against published experimental CNG pressure and apparent heat-release data, with mean deviations of 0.39 bar and 0.52 J/°CA, respectively. The baseline simulation predicted a peak in-cylinder pressure of 53.5 bar at approximately 11° ATDC and a maximum temperature of 2380 K at 21° ATDC. Peak apparent heat-release rate was 48.55 J/°CA, with 825.4 J total heat release and a 28° CA CA10–CA90 combustion duration. Gross indicated mean effective pressure was 4.97 bar, with 3.94 kW indicated power and 23.43% indicated thermal efficiency. CO, CO_2, NO and NO_2 formation was also examined. The study provides a documented numerical baseline for Nigerian-composition CNG combustion in an SIDI engine and a reference condition for subsequent parametric studies.

Keywords— compressed natural gas; Nigerian natural gas; spark-ignition direct injection; computational fluid dynamics; combustion

1 INTRODUCTION

The transportation sector remains a major contributor to global greenhouse-gas emissions, creating continued interest in lower-emission alternatives to conventional petroleum-derived fuels. Although electrification is progressing rapidly, the transition to electric mobility remains constrained in many developing regions by infrastructure, energy-system and economic considerations. These constraints have encouraged a maintained interest in alternative fuels that can be deployed using existing internal-combustion-engine technologies. Among these alternatives, natural gas is attractive because of its relatively high hydrogen-to-carbon ratio and its potential to reduce carbon dioxide and particulate emissions compared with conventional liquid hydrocarbon fuels (Chala et al., 2018). Compressed natural gas (CNG) can be used in spark-ignition engines and has therefore received considerable attention as a transition fuel for road transportation. Despite these advantages, the use of CNG in conventional spark-ignition engines presents challenges associated with its gaseous state and combustion characteristics. Unlike liquid gasoline, gaseous CNG occupies part of the intake charge volume when introduced through port fuel injection, reducing the amount of air inducted into the cylinder and consequently limiting volumetric efficiency and engine power (Jahirul et al., 2010). CNG also has a relatively low laminar flame speed and requires comparatively high ignition energy, which can influence combustion development and stability (Chala et al., 2018). Direct injection of CNG into the combustion chamber provides a means of mitigating the volumetric-efficiency penalty associated with port injection by introducing the fuel after the intake process. High-pressure direct

Corresponding Author: atoyeniran@oauife.edu.ng

Section C- MECHANICAL/MECHATRONICS ENGINEERING & RELATED SCIENCES

Can be cited as:

Adewole B. Z., Oyeniran A. T., Oni A. B., Fasogbon S. K., Adedoja A. M., Ohunakin O. S., and Asere A. A. (2026). A Numerical Characterisation of Nigerian-Composition CNG Combustion in a Spark-Ignition Direct-Injection Engine. FUOYE Journal of Engineering and Technology (FUOYE**JET**), **11(3), 472-480.** https://dx.doi.org/10.46792/fuoyejet.v11i3.1604

© 2026 The Author(s). Published by Faculty of Engineering, Federal University Oye-Ekiti.
This is an open access article under the CC BY NC license. (https://creativecommons.org/licenses/by-nc/4.0/)

injection also provides greater control over the timing and spatial distribution of the fuel, thereby influencing mixture formation and combustion. Experimental and numerical investigations have demonstrated the importance of injection strategy to the combustion and performance of direct-injected CNG engines (Aljamali et al., 2016; Choi et al.,2015; Choi et al., 2016).

The combustion behaviour of a direct-injection natural-gas engine is governed not only by the injection process and engine operating conditions but also by the composition of the fuel. Natural gas is not a single chemical species; its composition varies according to geographical location and source and may contain methane together with varying proportions of ethane, propane and heavier hydrocarbons (Chala et al., 2018). Such compositional variations can alter the thermochemical properties of the fuel and consequently affect ignition, flame propagation, heat release, combustion phasing and pollutant formation. Numerical studies have demonstrated the value of three-dimensional simulation for resolving the interaction between fuel injection, in-cylinder flow, turbulent flame propagation and combustion chemistry. G-equation approaches have, for example, been applied to natural-gas engine simulations (Liu and Dumitrescu, 2018), while CFD studies have examined the effects of mixture composition, EGR and hydrogen addition on natural-gas combustion (Baratta et al., 2020). Experimental work has also compared direct-injected CNG with other fuel-delivery systems and documented differences in combustion and emissions (Melaika et al., 2021).

The existing literature therefore provides substantial evidence that CNG can be successfully employed in spark-ignition engines and that direct injection offers important advantages for gaseous-fuel utilization. However, much of the available engine research represents CNG using methane or generic natural-gas formulations, while comparatively less attention has been given to detailed three-dimensional CFD characterisation using a natural-gas composition representative of a specific Nigerian gas source. This distinction is relevant because the composition of Nigerian natural gas varies between production locations, and the resulting fuel properties can influence predicted combustion and emissions. Natural gas from the Utorogu Gas Plant in Nigeria, for example, is predominantly methane but also contains appreciable quantities of ethane and smaller fractions of propane, butanes and pentanes (Sonibare and Akeredolu, 2006). Representing this composition in an engine simulation therefore provides a more geographically specific basis for assessing CNG combustion than a pure-methane representation.

Dandajeh and Ahmadu (2019) examined crank-angle-resolved cylinder pressure and engine-performance behaviour in an internal-combustion engine, while Isaac (2022) reviewed performance-related considerations in spark-ignition engines. More recently, Olugasa et al. (2026) investigated the performance and energy implications of a gaseous alternative fuel in a Nigerian engine-generator application. These studies reinforced the relevance of engine performance, combustion behaviour and locally applicable alternative-fuel research, but none directly addresses the three-dimensional CFD characterisation of Nigerian-composition CNG in a SIDI engine.

Three-dimensional CFD provides information that is difficult to obtain experimentally, including the spatial evolution of temperature, fuel distribution, flame propagation and pollutant formation. The present study consequently establishes a quantitative CFD baseline for Nigerian-composition CNG in a SIDI engine. The contribution is deliberately not framed as an optimization of injection timing or as a CNG–gasoline comparison. Instead, the study documents combustion phasing, temperature development, heat release, flame structure, gross indicated performance and major gaseous emissions under a defined early-injection, predominantly homogeneous-charge condition. The model is evaluated against published experimental CNG pressure and apparent heat-release data before the baseline results are interpreted. The resulting reference condition provides a basis for subsequent investigations of injection timing, engine speed, injection pressure, fuel-composition variation, knock behaviour and multi-cylinder implementation.

2 METHODOLOGY

2.1 Engine Geometry and Operating Conditions

A three-dimensional computational model of a single-cylinder research engine was developed using SolidWorks® and subsequently imported into ANSYS Forte 2021 R2 for the engine-cycle simulations. The model was based on a 0.5-L AVL single-cylinder research engine. Taking advantage of the geometric symmetry of the engine, one half of the cylinder was used as the computational domain, thereby reducing the computational requirements while retaining the relevant flow and combustion features. The computational geometry includes the intake and exhaust ports, intake and exhaust valves, centrally mounted fuel injector and spark-plug location. A sub-volume bounded by the cylinder head, cylinder liner and piston were defined within ANSYS Forte to represent the combustion chamber.

© 2026 The Author(s). Published by Faculty of Engineering, Federal University Oye-Ekiti.
This is an open access article under the CC BY NC license. (https://creativecommons.org/licenses/by-nc/4.0/)

http://.doi.org/10.46792/fuoyejet.v11i3.1604 engineering.fuoye.edu.ng/journal

The principal geometric parameters of the engine are a bore of 82 mm, stroke of 90 mm and connecting-rod length of 139.5 mm, giving a displacement of 0.5 dm^3. The engine has four valves and a compression ratio of 10:1. The valve events used in the model were an intake-valve opening at 364° BTDC, intake-valve closing at 142° BTDC, exhaust-valve opening at 575° BTDC and exhaust-valve closing at 363° BTDC. The principal engine specifications are summarized in Table 1.

Table 1. Engine geometry and baseline operating conditions.

Parameter	Value
Engine type	0.5-L AVL single-cylinder research engine
Bore	82 mm
Stroke	90 mm
Connecting-rod length	139.5 mm
Number of valves	4
Compression ratio	10:1
Engine speed	2000 rpm
Load	Wide-open throttle
CNG injection pressure	50 bar
Baseline start of injection	310° BTDC
Injected CNG mass	29 mg
Equivalence ratio at ignition	1.004

The present study was designed as a baseline CFD characterisation of Nigerian-composition CNG under a fixed engine operating condition. The engine was operated at 2000 rpm and wide-open throttle (WOT), with a CNG injection pressure of 50 bar. The baseline CNG case employed a start of injection of 310° BTDC, which was selected to provide a predominantly homogeneous charge condition before ignition and was therefore used as the reference condition for the combustion, performance and emission analyses presented in this study. The corresponding injected CNG mass was 29 mg, giving an equivalence ratio of 1.004 at ignition.

Other injection timings were considered during development of the broader numerical investigation; however, they are not analyzed in the present study. The objective of the present work is to establish the combustion, performance and emission characteristics of Nigerian-composition CNG under a defined baseline homogeneous-charge condition rather than to perform an injection-timing sensitivity study. Consequently, the effects of injection timing, engine speed and load are outside the scope of the present analysis and are identified as areas for further investigation.

2.2 Fuel Composition and CNG Surrogate

The CNG used in the present study was formulated to represent the composition of natural gas reported for the Utorogu Gas Plant in Nigeria. The reported gas consists predominantly of methane, with smaller fractions of ethane, propane, butanes and pentanes. The molar composition adopted as the basis for the fuel representation is presented in Table 2.

To account for the influence of fuel composition while maintaining a computationally tractable chemical description, a multi-component natural-gas mechanism from the ANSYS Model Fuel Library (MFL) was employed. The mechanism is derived from the full GaseousFuels_C0-C6_NOx mechanism and provides a reduced representation of natural-gas combustion using methane, ethane and n-butane as the principal fuel components. In accordance with the surrogate formulation used in the model, hydrocarbons heavier than C2 were lumped into the n-butane component. Thus, the reported Utorogu gas composition was used as the physical basis for the fuel formulation, while the reduced three-component representation was used in the CFD calculation.

The selected natural-gas mechanism was developed for conditions covering pressures of 10–100 bar, temperatures of 800–2000 K, equivalence ratios of 0.4–3.0 and exhaust-gas-recirculation levels of 0–20%. The parent gaseous-fuel mechanism has been evaluated against shock-tube ignition data for methane/ethane/hydrogen mixtures (Herzler and Naumann, 2009). These ranges encompass the principal thermodynamic and mixture conditions encountered during the present engine-cycle simulation. The reported molar composition of the Utorogu natural gas is given in Table 2.

Table 2. Molar composition of natural gas at the Utorogu Gas Plant, Nigeria (Sonibare and Akeredolu, 2006).

Species	Molar composition (%)
Methane (CH_4)	90.12
Ethane (C_2H_6)	6.94
Propane (C_3H_8)	2.09
n-Butane (n-C_4H_{10})	0.361
i-Butane (i-C_4H_{10})	0.414
n-Pentane (n-C_5H_{12})	0.005
i-Pentane (i-C_5H_{12})	0.007

The resulting CNG representation was used consistently for the baseline Nigerian-CNG simulation. This approach preserves the principal compositional characteristics of the Nigerian natural gas while avoiding the computational expense associated with representing every hydrocarbon component explicitly in the engine simulation.

2.3 Computational Geometry and Mesh

The three-dimensional engine geometry was discretised using the automatic meshing capability of ANSYS Forte 2021 R2. The computational domain exploited the geometric symmetry of the single-cylinder engine, with one half of the engine retained for the simulations. The domain comprised the cylinder, piston, cylinder head, intake and exhaust ports, valves, centrally mounted fuel injector and spark-plug region. A sub-volume bounded by the cylinder head, cylinder liner and piston were defined within the CFD model to represent the combustion chamber. Table 3, shows the meshing details.

Table 3. Meshing Details

Parameter	Specification
Mesh type	Adaptive moving mesh
Global mesh size	0.4 cm

© 2026 The Author(s). Published by Faculty of Engineering, Federal University Oye-Ekiti.
This is an open access article under the CC BY NC license. (https://creativecommons.org/licenses/by-nc/4.0/)

http://.doi.org/10.46792/fuoyejet.v11i3.1604 engineering.fuoye.edu.ng/journal

Combustion chamber mesh	0.2 cm
Wall/valve refinement	0.1 cm
Ignition-region refinement	0.05 cm within 0.6 cm radius
Ignition refinement period	40° BTDC–40° ATDC
Mesh update interval	0.1 ms
Maximum cells	≈240,000
Adaptive refinement	Temperature, velocity, fuel-vapour and G-variable gradients
AMR criterion	Standard-deviation-based gradient threshold
Grid-independence	Not demonstrated; baseline mesh

3 GOVERNING EQUATIONS AND COMPUTATIONAL MODELS

The in-cylinder flow and combustion processes were modelled by solving the conservation equations for chemical species, total mass, momentum and energy, together with an equation of state for the gas mixture. The formulation accounts for the transport of individual chemical species, turbulent momentum transfer, molecular diffusion, heat transfer, chemical reaction and fuel-injection source terms. The gas phase was assumed to behave as an ideal gas, while the fluid was treated as Newtonian. Molecular mass diffusion and thermal diffusion were represented using Fick's and Fourier's laws, respectively. These assumptions and governing equations form the basis of the ANSYS Forte formulation used in the present engine-cycle simulations.

3.1 Species, Mass, Momentum and Energy Conservation

The conservation equation for each chemical species kk is expressed as

$$\partial \varrho_k/\partial t + \nabla\cdot(\varrho u\, y_k) = \nabla\cdot[\varrho D \nabla y_k] + \nabla\cdot\Phi + \dot{\varrho}_k^{c} + \dot{\varrho}_k^{s}, \quad k = 1, \ldots, K \quad (1)$$

where ρ is the mean mixture density, ρ_k is the mean density of species k, u is the mean velocity vector, y_k is the mass fraction of species k, D is the molecular diffusion coefficient, Φ represents turbulent/ensemble-averaged species transport, $\dot{\varrho}_k^{c}$ is the source term resulting from chemical reactions and $\dot{\rho}_k^{s}$ is the source term associated with fuel injection.

The species conservation equations therefore account for the transport and transformation of the individual constituents of the reacting mixture throughout the engine cycle. Chemical reaction and fuel-injection source terms couple the species equations with the combustion and injection models described in the subsequent sections.

3.1.1 Conservation of Mass

The total gas-phase mass conservation equation is obtained by summing the individual species equations and is given by

$$\partial \varrho/\partial t + \nabla\cdot(\varrho u) = \varrho^{s} \quad (2)$$

where ϱ^{s} represents the mass source associated with fuel injection.

This formulation accounts for the addition of fuel to the computational domain during the injection process while maintaining conservation of the total gas-phase mass.

3.1.2 Momentum Conservation

The momentum conservation equation is expressed as

$$\partial(\varrho u)/\partial t + \nabla\cdot(\varrho u u) = -\nabla p + \nabla\cdot\sigma - \nabla\cdot\Gamma + F^{s} + \varrho g \quad (3)$$

where p is the mean pressure, σ is the viscous stress tensor, Γ represents the Reynolds-stress contribution associated with turbulent momentum transport, F^{s} is the momentum source associated with fuel injection, and g is the gravitational acceleration.

The momentum equation is therefore coupled to the turbulence and injection models, allowing the effects of turbulent transport and fuel addition on the in-cylinder flow field to be represented.

3.1.3 Energy Conservation

The conservation equation for the mean specific internal energy is given by

$$\partial(\varrho I)/\partial t + \nabla\cdot(\varrho u I) = -p\nabla\cdot u - \nabla\cdot J - \nabla\cdot H + \varrho\varepsilon + Q^{c} + Q^{s} - Q\text{rad} \quad (4)$$

where I is the mean specific internal energy, J represents the heat-flux contribution associated with molecular transport, H represents the enthalpy transport contribution, $\rho\varepsilon$ represents turbulent dissipation, Q^{c} is the chemical heat-release source term, Q^{s} is the energy source associated with fuel injection and $Qrad$ represents radiative heat loss.

The energy equation provides the coupling between the combustion process and the thermodynamic state of the in-cylinder charge. Chemical heat release changes the temperature and pressure fields, while heat transfer and fuel injection influence the evolution of the mixture energy throughout the engine cycle.

3.1.4 Equation of State

The thermodynamic state of the gas mixture was determined using an ideal-gas equation of state based on the partial pressures of the constituent species. The mixture pressure is expressed as

$$p = R_u\, T\, \Sigma_k(\varrho_k/W_k) \quad (5)$$

where R_u is the universal gas constant, T is the mean mixture temperature and W_k is the molecular weight of species k.

The ideal-gas formulation was applied to the multicomponent reacting mixture throughout the engine-cycle simulation. This allows the instantaneous pressure, temperature and species composition to remain coupled through the thermodynamic properties of the mixture.

3.2 Simulation Models

The simulation was done based on the models in Table 4.

Table 4. Simulation Models

Model/Parameter	Baseline specification
Turbulence model	RANS with RNG k–ε model
Turbulence application	In-cylinder flow, fuel–air mixing and turbulent flame propagation

© 2026 The Author(s). Published by Faculty of Engineering, Federal University Oye-Ekiti.
This is an open access article under the CC BY NC license. (https://creativecommons.org/licenses/by-nc/4.0/)

http://.doi.org/10.46792/fuoyejet.v11i3.1604 engineering.fuoye.edu.ng/journal

CNG injection model	ANSYS Forte gaseous-sphere injection model
Injector configuration	10-hole direct injector
Injection pressure	50 bar
Discharge coefficient	0.5
Spray cone angle	14°
Injection duration	15.7° crank angle
Sauter Mean Diameter (SMD)	10 μm
Droplet collision model	Disabled
KH breakup SMD conservation	Disabled
RT distance constant	0.2
Combustion treatment	Partially premixed turbulent combustion
Ignition model	Discrete Particle Ignition Kernel (DPIK)
Spark timing	18° BTDC
Spark duration	10° crank angle
Ignition particles	3,000 flame particles
Initial kernel radius	0.25 mm
Energy release rate	20 J/s
Spark-energy efficiency	50%
Flame propagation model	Level-set G-equation
G-equation activation	Flame kernel radius = 1 mm
Laminar flame speed	Peters (2000) correlation; dependent on fuel composition, pressure and temperature
Heat-release treatment	Flame propagation as primary heat-release mechanism, coupled with chemical kinetics
Flame temperature	Adiabatic flame temperature under constant-pressure assumption
Flame quenching criterion	$l_k < l_\delta$
Quenching parameters	Kolmogorov length scale, l_k and laminar flame inner-layer thickness, l_δ

3.5 Boundary and Initial Conditions

The boundary and initial conditions were specified to represent the gas-exchange, compression, combustion and expansion processes of the engine over the simulated cycle. The engine-cycle simulation employed moving-wall and open-boundary conditions with prescribed surface temperatures and residual-gas initialization. The governing equations were solved using a finite-volume ALE formulation with operator splitting, modified SIMPLE pressure–velocity coupling, quasi-second-order upwinding, and dynamic cell clustering to reduce the computational cost of detailed chemistry. The boundary and initial conditions were according to Table 5.

Table 5. Boundary and Initial Conditions

Parameter	Baseline specification
Boundary treatment	Moving walls, open intake/exhaust boundaries, and symmetry plane
Wall heat transfer	Han–Reitz heat-transfer model
Intake boundary	1 bar, 313 K; air composition: 76.7% N_2, 23.3% O_2
Exhaust boundary	1 bar outflow
Piston motion	Moving wall; 9.0 cm stroke, 13.95 cm connecting rod
Cylinder liner temperature	500 K
Cylinder-head, Piston and Spark- plug temperature	485 K
Intake-valve temperature	400 K
Exhaust-valve temperature	777 K
Valve treatment	Moving boundaries with prescribed lift profiles
Open-boundary turbulence	TKE = 10,000 cm²/s²; length scale = 1 cm
Symmetry condition	Half-engine computational domain
Initial intake state	313 K, 1.00 bar; 76.7% N_2, 23.3% O_2
Initial cylinder state	1070 K, 1.05 bar; residual gas: 15.6% CO_2, 12.0% H_2O, 72.4% N_2
Initial exhaust state	1070 K, 1.00 bar; residual-gas composition
Initial velocity	0 m/s in all regions
Initial turbulence	TKE = 10,000 cm²/s²; length scale = 1 cm
Spatial discretisation	Finite control-volume method
Temporal treatment	Operator splitting
Moving mesh formulation	Arbitrary-Lagrangian-Eulerian (ALE)
Pressure–velocity coupling	Modified SIMPLE algorithm
Convective discretisation	Quasi-second-order upwind
Chemistry solver	ANSYS Forte chemistry solver
Chemistry acceleration	Dynamic cell clustering (DCC)
DCC variables	Temperature and equivalence ratio
DCC tolerances	10 K and 0.05, respectively
Engine speed	2000 rpm
Simulation interval	IVO to EVO
Initial timestep	5.0×10^{-7}s
Maximum crank-angle increment	1.1° CA
Maximum timestep	5.0×10^{-6}s
Chemistry activation	After first spark for $T > 600$ K; explicitly active from 70° BTDC to 140° ATDC

3.7 Model Validation

As shown in Figure 1, the model was validated against the experimental results of Melaika et al. (2021) using in-cylinder pressure and AHRR profiles. The simulations reproduced the experimental combustion phasing and heat-release behaviour, with mean deviations of 0.39 bar and 0.52 J/°CA, respectively. The slight overprediction of peak pressure was attributed primarily to the exclusion of friction losses. Overall, the validation supports the application of the computational framework to the present CNG engine analysis.

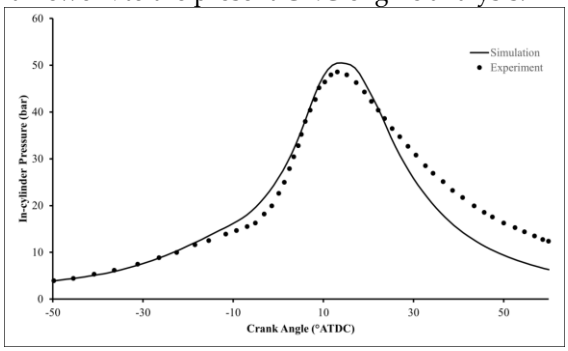

Fig. 1. Comparison of experimental and simulated CNG in-cylinder pressure and apparent heat-release rate.

4 RESULTS AND DISCUSSION

The baseline case represents Nigerian-composition CNG injected at 310° BTDC into the 0.5-L SIDI research engine at 2000 rpm, wide-open throttle and 50 bar injection pressure. The early injection strategy provided sufficient premixing time before the 18° BTDC spark and therefore served as the predominantly homogeneous reference condition. The discussion below focuses on the principal

© 2026 The Author(s). Published by Faculty of Engineering, Federal University Oye-Ekiti.
This is an open access article under the CC BY NC license. (https://creativecommons.org/licenses/by-nc/4.0/)

http://.doi.org/10.46792/fuoyejet.v11i3.1604 engineering.fuoye.edu.ng/journal

combustion, performance and emission responses while retaining the original CFD figures and tables.

4.1 Baseline Combustion Characteristics

4.1.1 In-cylinder Pressure and Combustion Phasing

Figure 2 shows a peak in-cylinder pressure of 53.5 bar at approximately 11° ATDC. The post-TDC maximum indicates that a substantial fraction of the heat release occurs close to TDC and early expansion, allowing combustion energy to contribute positively to piston work. The pressure peak is also consistent with finite-duration SI combustion: although the spark occurs at 18° BTDC, flame-kernel growth and turbulent propagation delay completion of the main heat-release event. The validated CFD framework reproduced the experimental pressure behaviour with a mean deviation of 0.39 bar (Fig. 1), supporting its use for baseline characterisation (Melaika et al., 2021).

The principal combustion consequence is the phasing of the pressure maximum rather than the magnitude alone. A peak shortly after TDC indicates that combustion is neither excessively advanced nor strongly delayed for the specified baseline. This behaviour is consistent with the finite-rate flame propagation represented by the DPIK/G-equation framework and with previous natural-gas CFD studies using G-equation-based combustion modelling (Liu & Dumitrescu, 2018; Choi et al., 2016).

4.1.2 In-cylinder Temperature and Thermal Development

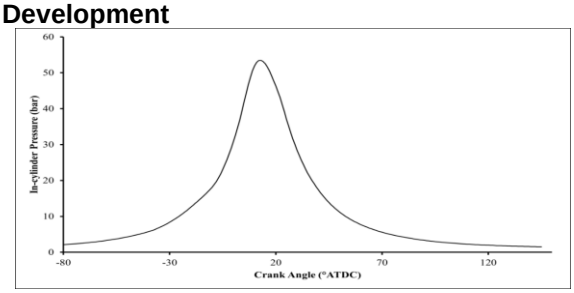

Fig. 2. Predicted in-cylinder pressure for baseline homogeneous CNG combustion.

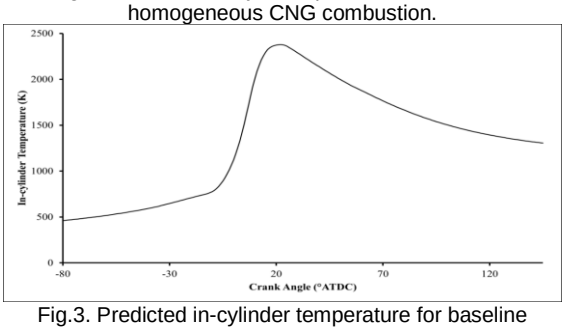

Fig.3. Predicted in-cylinder temperature for baseline homogeneous CNG combustion.

Figure 3 shows a maximum in-cylinder temperature of approximately 2380 K at 21° ATDC, about 10° CA after the pressure maximum. The delayed temperature peak indicates that chemical heat release continues into early expansion even as cylinder volume increases and pressure begin to decline. The temperature field therefore confirms that combustion is still thermally active after the pressure peak. The 2380 K level also identifies the high-temperature region associated with temperature-sensitive pollutant chemistry, particularly nitrogen-oxide formation.

The temporal separation between the pressure and temperature maxima is an important feature of the baseline case. Pressure reflects the combined effects of heat release and instantaneous cylinder volume, whereas temperature follows the thermal development of the reacting charge. Consequently, the later temperature maximum is physically consistent with continued oxidation during early expansion and provides a basis for interpreting the NO distribution shown in Figure 9 and 10.

4.1.3 Apparent Heat-Release Rate

Figure 4 gives a peak apparent heat-release rate (AHRR) of 48.55 J/°CA. The rapid rise identifies the principal combustion phase, while the subsequent decline indicates a reduction in the rate of energy release as the unburned mixture is consumed. The AHRR peak occurs close to the pressure maximum, demonstrating the strong coupling between heat release and cylinder-pressure development during the main combustion event.

Because AHRR is derived from the pressure history, it should be interpreted primarily as a combustion-phasing and heat-release-intensity diagnostic rather than as a direct chemical source term. In the present calculation, $\gamma = 1.35$ was used in the pressure-based formulation. The decline-region fluctuations therefore do not, by themselves, demonstrate incomplete combustion. The AHRR prediction also showed good agreement with the validation data, with a mean deviation of 0.52 J/°CA.

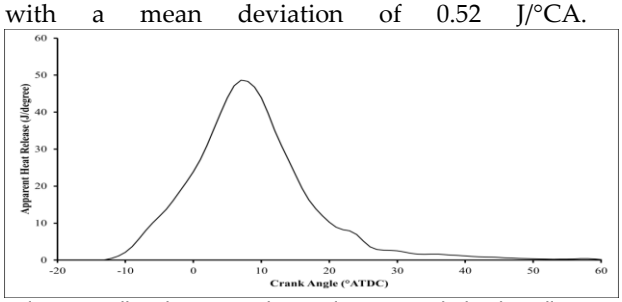

Fig. 4. Predicted apparent heat-release rate during baseline CNG combustion.

4.1.4 Flame Development and Spatial Temperature Distribution

Figure 5 shows a spatially non-uniform temperature field during early expansion. Despite the early-injection strategy and predominantly homogeneous charge, the flame does not propagate uniformly throughout the chamber. Faster development is observed toward the spark-plug/intake-valve side, whereas propagation is slower near the cylinder wall. This pattern indicates that local flow structure, turbulence and thermochemical state influence the instantaneous flame-development rate, even when large-scale premixing has been achieved.

© 2026 The Author(s). Published by Faculty of Engineering, Federal University Oye-Ekiti.
This is an open access article under the CC BY NC license. (https://creativecommons.org/licenses/by-nc/4.0/)

http://.doi.org/10.46792/fuoyejet.v11i3.1604 engineering.fuoye.edu.ng/journal

The observed spatial variation is consistent with the established role of turbulence in wrinkling and transporting the flame front (Peters, 2000; Han & Reitz, 1995). However, the temperature contour alone does not establish a causal relationship between turbulence intensity and flame speed; the interpretation is therefore limited to the spatial correlation visible in the CFD field. The high-temperature regions shown in Figure 6 also provide the spatial basis for the NO distribution discussed later.

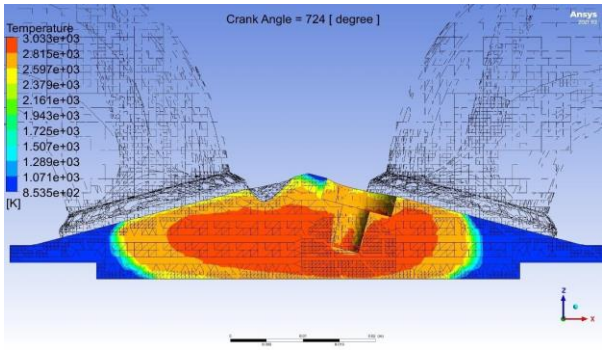

Fig. 6. Predicted in-cylinder temperature distribution during the early expansion stroke.

4.1.5 Total Heat Release, Combustion Duration and Efficiency

Overall, the combustion results in Table 6 establish a coherent baseline: 53.5 bar peak pressure at 11° ATDC, 2380 K peak temperature at 21° ATDC, 48.55 J/°CA peak AHRR, 825.4 J total heat release, 28° CA CA10–CA90 duration and 99.8% predicted combustion efficiency. These quantities are the principal reference values for subsequent parametric studies.

Table 6. Summary of baseline CNG combustion characteristics.

Parameter	Predicted value
Maximum in-cylinder pressure	53.5 bar
Crank angle of maximum pressure	≈11° ATDC
Maximum in-cylinder temperature	2380 K
Crank angle of maximum temperature	21° ATDC
Peak apparent heat-release rate	48.55 J/°CA
Total heat released	825.4 J
Combustion duration, CA10–CA90	28° CA
Combustion efficiency	99.8%

4.2 Baseline Indicated Performance

The baseline combustion cycle produced a predicted IMEP of 4.97 bar, gross indicated power of 3.94 kW at 2000 rpm, ISFC of 335.12 g/kWh, and indicated thermal efficiency of 23.43%. The IMEP reflects the net indicated work obtained from the simulated compression and expansion strokes, while the gross indicated power represents the corresponding pressure–volume work converted to power. The post-TDC pressure peak supports positive indicated work because a substantial portion of the heat release occurs during the expansion stroke. Since frictional and drivetrain losses were excluded from the CFD model, these values represent gross indicated rather than brake-level performance. The predicted thermal efficiency indicates the fraction of CNG chemical energy converted to indicated work under the specified operating condition and is influenced by combustion phasing, total heat release, wall heat transfer and indicated work. Consequently, the ISFC and thermal-efficiency values should be interpreted within the CFD modelling framework and operating condition rather than directly compared with brake-performance data from production engines.

4.3 Baseline Emission Characteristics

The CFD model also predicted the spatial and temporal development of CO, CO_2, NO and NO_2 during combustion. These results are retained as model-predicted emission characteristics, rather than being presented as independently validated emission measurements.

This distinction is important because the validation evidence primarily concerns in-cylinder pressure and AHRR, with reported mean deviations of 0.39 bar and 0.52 J/degree, respectively. No equivalent experimental validation dataset for the predicted species concentrations is available.

4.3.1 CO and CO_2 Formation

Figures 6 shows that CO begins to form at about 13° BTDC, reaches a maximum near 20° ATDC and decreases thereafter to approximately 5 mg at exhaust-valve opening. The early CO concentration is concentrated around the ignition region, where partially oxidised intermediates are first produced. The subsequent decline is consistent with progressive oxidation as combustion proceeds through the chamber. In contrast, CO_2 rises rapidly after ignition and reaches a maximum near 21° ATDC, with approximately 23 mg present at EVO.

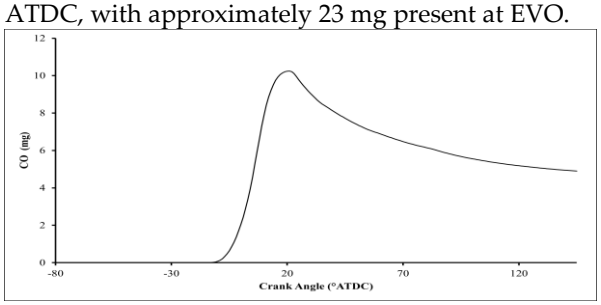

(a)

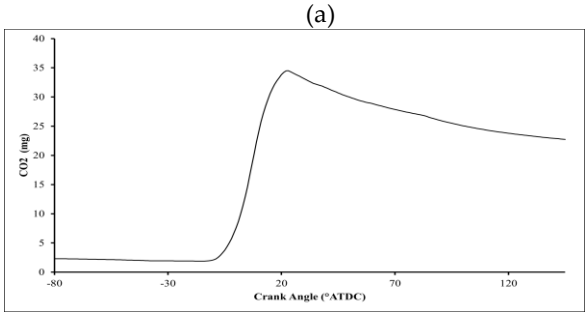

(b)

Fig. 6. Predicted temporal evolution of (a) CO and (b) CO_2 within the combustion chamber.

The spatial evolution in Figure 7 follows the advancing flame region, while the temporal trends

© 2026 The Author(s). Published by Faculty of Engineering, Federal University Oye-Ekiti.
This is an open access article under the CC BY NC license. (https://creativecommons.org/licenses/by-nc/4.0/)

http://.doi.org/10.46792/fuoyejet.v11i3.1604 engineering.fuoye.edu.ng/journal

in Figure 8 show the progressive conversion of carbon-containing intermediates toward more fully oxidised products. The simultaneous decrease in CO and increase in CO_2 after the main combustion phase are therefore consistent with continued oxidation during early expansion. These concentrations remain dependent on the chemistry model and should not be interpreted as direct experimental exhaust measurements.

4.3.2 NO and NO_2 Formation

Figures 7 show substantially smaller predicted nitrogen-oxide quantities than the CO and CO_2 levels. NO rises during the high-temperature combustion period and reaches approximately 0.17 mg at around 14° ATDC, whereas the maximum NO_2 quantity is only about 0.48 μg before declining toward negligible levels.

The NO maximum occurs shortly after the 11° ATDC pressure peak and before the 21° ATDC temperature maximum, indicating that NO formation is governed by the local thermal and chemical history rather than by pressure alone. The spatial NO field in Figure 9 is concentrated in the hottest combustion regions identified in Figure 6, which is consistent with the strong temperature dependence of thermal-NO pathways.

The much smaller NO_2 prediction indicates that NO is the dominant nitrogen-oxide species in the simulated combustion field. However, because no equivalent experimental NO/NO_2 measurements are available, Figures 9 and 10 should be interpreted as model-based spatial and temporal predictions rather than validated emission levels.

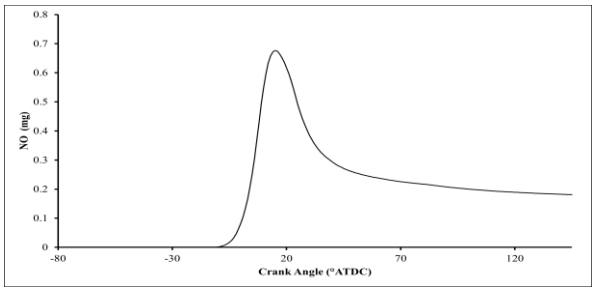

(a)

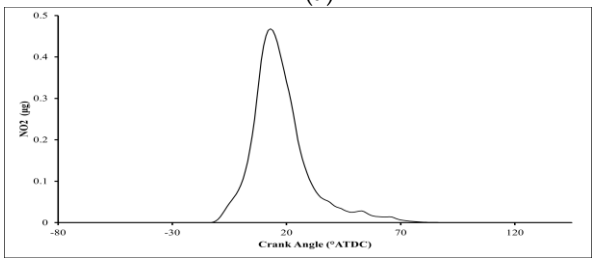

(b)

Fig. 10. Predicted temporal evolution of (a) NO and (b) NO_2 within the combustion chamber.

4.4 Integrated Interpretation of the Baseline Case

The baseline results form a consistent combustion sequence. Early CNG injection at 310° BTDC provides premixing time before the 18° BTDC spark; the resulting flame develops through the turbulent in-cylinder flow, produces the main heat-release event around TDC and continues into early expansion. Accordingly, the maximum pressure occurs at 11° ATDC, the maximum temperature at 21° ATDC, and the CA10–CA90 combustion duration is 28° CA.

The 48.55 J/°CA peak AHRR and 825.4 J total heat release quantify the intensity and integrated energy release of the combustion event. The spatial field in Figure 6 further shows that a nominally homogeneous charge does not imply uniform local combustion rates; local turbulence and flow structure remain important to flame development (Peters, 2000; Han & Reitz, 1995).

These combustion characteristics determine the predicted indicated performance: 4.97 bar IMEP, 3.94 kW gross indicated power, 335.12 g/kWh ISFC and 23.43% indicated thermal efficiency. The values are gross indicated quantities because frictional losses were omitted. Similar engine studies also demonstrate the importance of clearly distinguishing operating conditions and performance definitions when interpreting alternative-fuel engine results (Dandajeh & Ahmadu, 2019; Olugasa et al., 2026).

The emission fields follow the same combustion structure. CO peaks during the active oxidation period and decreases thereafter, while CO_2 continues to build toward the later combustion stages (Figure 6). NO is concentrated in the high-temperature regions and peaks after the pressure maximum, whereas NO_2 remains very small (Figure 7). The emission results therefore provide useful mechanistic information but remain unvalidated species predictions.

5 CONCLUSIONS

This study establishes a three-dimensional CFD baseline for Nigerian-composition CNG combustion in a spark-ignition direct-injection research engine. The study is deliberately restricted to a defined early-injection, predominantly homogeneous-charge condition and is intended as a reference case rather than an optimization study.

At 2000 rpm, wide-open throttle, 50 bar injection pressure and 310° BTDC start of injection, the model predicts a peak in-cylinder pressure of 53.5 bar at approximately 11° ATDC and a maximum temperature of 2380 K at 21° ATDC. The peak AHRR is 48.55 J/°CA, total heat release is 825.4 J and the CA10–CA90 combustion duration is 28° CA. The resulting gross indicated performance is 4.97 bar IMEP, 3.94 kW indicated power, 335.12 g/kWh ISFC and 23.43% indicated thermal efficiency.

The validation against published experimental CNG data gives mean deviations of 0.39 bar for in-cylinder pressure and 0.52 J/°CA for AHRR, supporting the use of the computational framework

© 2026 The Author(s). Published by Faculty of Engineering, Federal University Oye-Ekiti.
This is an open access article under the CC BY NC license. (https://creativecommons.org/licenses/by-nc/4.0/)

http://.doi.org/10.46792/fuoyejet.v11i3.1604 engineering.fuoye.edu.ng/journal

for baseline combustion characterization. The predicted emission fields provide additional spatial and temporal information on CO, CO_2, NO and NO_2 formation, but these species predictions remain unvalidated by equivalent experimental measurements. The principal contribution is a documented Nigerian-composition CNG CFD reference case that can support future studies of injection timing, engine speed, injection pressure, fuel-composition variation, knock behaviour and multi-cylinder implementation. Future work should prioritize mesh and timestep independence, parameters sensitivity study and uncertainty analysis, expanded experimental validation of emissions, and extension of the model to a wider range of operating conditions and multi-cylinder configurations.

ACKNOWLEDGEMENT

The authors acknowledge the computational and institutional support provided during the original study. This publication has been produced with financial support of Nigeria Tertiary Education Trust Fund (TETFUND) National Research Foundation (NRF) on "Engine Performance and Air Quality Assessment of a Compressed Natural Gas Retrofitted Vehicle, Grant No. 00017, 2021. The authors appreciated and acknowledged the computational support of the Cybersecurity Laboratory of the African Centre of Excellence (ACE) under the World Bank Project Grant No: P169064 at the Obafemi Awolowo University, Ile-Ife, Nigeria.

CONFLICTS OF INTEREST

The authors declare no known conflict of interest.

REFERENCES

Aljamali, S., Abdullah, S., Mahmood, W. M. F., & Ali, Y. (2016). The effect of injection timings on performance and emissions of compressed natural-gas direct injection engine. *Journal of Combustion, 2016*, Article ID 6501462. doi:10.1155/2016/6501462

Baratta, M., Chiriches, S., Goel, P., & Misul, D. (2020). CFD modelling of natural gas combustion in IC engines under different EGR dilution and H_2-doping conditions. *Transportation Engineering, 2*, 100018. doi:10.1016/j.treng.2020.100018

Chala, G. T., Abd Aziz, A. R., & Hagos, F. Y. (2018). Natural gas engine technologies: Challenges and energy sustainability issue. *Energies, 11*(11), 2934. doi:10.3390/en11112934

Choi, M., Lee, S., & Park, S. (2015). Numerical and experimental study of gaseous fuel injection for CNG direct injection. *Fuel, 140*, 693–700. doi:10.1016/j.fuel.2014.10.018

Choi, M., Song, J., & Park, S. (2016). Modeling of the fuel injection and combustion process in a CNG direct injection engine. *Fuel, 179*, 168–178. doi:10.1016/j.fuel.2016.03.099

Dandajeh, H. A., & Ahmadu, T. O. (2019). Engine performance of a Gardener compression ignition engine using rapeseed methyl ester. *FUOYE Journal of Engineering and Technology, 4*(2), 126–130. doi:10.46792/fuoyejet.v4i2.325

Fan, L., & Reitz, R. D. (2000). Development of an ignition and combustion model for spark-ignition engines. *SAE Transactions, 109*, 1977–1989. SAE Technical Paper 2000-01-2809.

Han, Z., & Reitz, R. D. (1995). Turbulence modeling of internal combustion engines using RNG k-ε models. *Combustion Science and Technology, 106*(4–6), 267–295. doi:10.1080/00102209508907782

Herzler, J., & Naumann, C. (2009). Shock-tube study of the ignition of methane/ethane/hydrogen mixtures with hydrogen contents from 0% to 100% at different pressures. *Proceedings of the Combustion Institute, 32*, 213–220.

Hessel, R. P., Aceves, S. M., & Flowers, D. L. (2006). Gaseous fuel injection modeling using a gaseous sphere injection methodology. SAE Technical Paper 2006-01-3265. doi:10.4271/2006-01-3265

Isaac, F. O. (2022). A review of coating methods and their applications in compression and spark-ignition engines for enhanced performance. *FUOYE Journal of Engineering and Technology, 7*(2), 217–221. doi:10.46792/fuoyejet.v7i2.810

Jahirul, M. I., Masjuki, H. H., Saidur, R., Kalam, M. A., Jayed, M. H., & Wazed, M. A. (2010). Comparative engine performance and emission analysis of CNG and gasoline in a retrofitted car engine. *Applied Thermal Engineering, 30*(14–15), 2219–2226. doi:10.1016/j.applthermaleng.2010.05.037

Liang, L., & Reitz, R. D. (2006). Spark ignition engine combustion modeling using a level set method with detailed chemistry. SAE Technical Paper 2006-01-0243. doi:10.4271/2006-01-0243

Liu, J., & Dumitrescu, C. E. (2018). 3D CFD simulation of a CI engine converted to SI natural gas operation using the G-equation. *Fuel, 232*, 833–844. doi:10.1016/j.fuel.2018.05.159

Melaika, M., Herbillon, G., & Dahlander, P. (2021). Spark ignition engine performance, standard emissions and particulates using GDI, PFI-CNG and DI-CNG systems. *Fuel, 293*, 120454. doi:10.1016/j.fuel.2021.120454

Olugasa, T. T., Akubueze, I. Ch., & Bolade, J. S. (2026). Energy, exergy and techno-economic analysis of a biogas powered generating set. *FUOYE Journal of Engineering and Technology, 11*(1), 115–122.

Peters, N. (2000). *Turbulent combustion*. Cambridge University Press. doi:10.1017/CBO9780511612701

Sonibare, J. A., & Akeredolu, F. A. (2006). Natural gas domestic market development for total elimination of routine flares in Nigeria's upstream petroleum operations. *Energy Policy, 34*(6), 743–753. doi:10.1016/j.enpol.2004.07.006

Tan, Z. C., Kong, S.-C., & Reitz, R. D. (2003). Modeling premixed and direct injection SI engine combustion using the G-equation model. SAE Technical Paper 2003-01-1843.

Yakhot, V., & Orszag, S. A. (1986). Renormalization group analysis of turbulence. I. Basic theory. *Journal of Scientific Computing, 1*(1), 1–51. doi:10.1007/BF01061452

© 2026 The Author(s). Published by Faculty of Engineering, Federal University Oye-Ekiti.
This is an open access article under the CC BY NC license. (https://creativecommons.org/licenses/by-nc/4.0/)